Small Island Effects in DYNAMO and Their Impact on Large-Scale Budget Analyses

PAUL E. CIESIELSKI[a] AND RICHARD H. JOHNSON[a]

[a] *Department of Atmospheric Science, Colorado State University, Fort Collins, Colorado*

(Manuscript received 15 October 2020, in final form 9 March 2021)

ABSTRACT: During the Dynamics of the MJO (DYNAMO) field campaign, radiosonde launches were regularly conducted from three small islands/atolls (Malé and Gan, Maldives, and Diego Garcia, British Indian Ocean Territory) as part of a large-scale sounding network. Comparison of island upsondes with nearby and near-contemporaneous dropsondes over the ocean provides evidence for the magnitude and scope of the islands' influence on the surrounding atmosphere and on the island upsonde profiles. The island's impact on the upsonde data is most prominent in the lowest 200 m. Noting that the vertical gradients of temperature, moisture, and winds over the ocean are generally constant in the lowest 0.5 km of dropsondes, a simple procedure was constructed to adjust the upsonde profiles in the lowest few hundred meters to resemble the atmospheric structures over the open ocean. This procedure was applied to the soundings from the three islands mentioned above for the October–December 2011 period of DYNAMO. As a result of this procedure, the adjusted diurnal cycle amplitude of surface temperature is reduced fivefold, resembling that over the ocean, and low-level wind speeds are increased in ~90% of the island soundings. Examination of the impact of these sounding adjustments shows that dynamical and budget fields are primarily affected by adjustments to the wind field, whereas convective parameters are sensitive to the adjustments in thermodynamic fields. Although the impact of the adjustments is generally small (on the order of a few percent), intraseasonal wind regime changes result in some systematic variations in divergence and vertical motion over the sounding arrays.

KEYWORDS: Marine boundary layer; Dropsondes; Soundings

1. Introduction

Islands can have a wide range of impacts on their surrounding atmosphere, depending on their size and topographic features. When stratified flow is blocked by larger islands with high topography such as Hawaii, Sri Lanka, and Sumatra, significant flow blocking and lee wake generation is likely (Smith and Grubisic 1993; Fine et al. 2016; Ciesielski et al. 2014b). In fact, using 2.5 years of model reanalyses, Fine et al. (2016) found that 25% of the tropical cyclones that formed in this period over the Indian Ocean originated from wake vortices shed downstream of significant topographic features in the "Maritime Continent." A second significant impact islands have on their circulation is the generation of convection due to the convergence of coastal sea and land breezes with the ambient flow. Mori et al. (2004) demonstrated how such convergence leads to an eastward-migrating peak in rainfall over Sumatra Island during the day and a westward-migrating offshore peak west of Sumatra during the nighttime hours. While the heating of small islands generates much weaker land–sea-breeze circulations, such effects are capable of producing precipitation in the vicinity of the islands (Wang and Sobel 2017), as well as organized circulations and cloud fields downstream of the islands. For example, cloud plumes are frequently observed over 100 km downwind of Nauru, a very small island (5 km in diameter) in the equatorial west Pacific with no topographic feature over 30 m (Matthews et al. 2007). Being an active Atmospheric Radiation Measurement (ARM) site for many years, the impact of the Nauru island on the ARM observations has received considerable attention (McFarlane et al. 2005). In quantifying the island's impact, Long and McFarlane (2011) found an overall 2% daylight average increase in low-level cloud occurrence and decrease in downwelling surface shortwave radiation in the ARM measurements but noted that over certain shorter periods these impacts were substantially larger.

A key observing system in the Dynamics of MJO (DYNAMO)/Cooperative Indian Ocean Experiment on Intraseasonal Variability in the Year 2011 (CINDY2011)/ARM MJO Investigation Experiment (AMIE) field campaign (hereinafter referred to as DYNAMO) was an atmospheric sounding network consisting of two quadrilateral arrays located on either side of the equator over the central Indian Ocean (Yoneyama et al. 2013). This core array, shown in Fig. 1, consisted of six sounding sites, the three westernmost being small islands/atolls, the eastern sites being Colombo, Sri Lanka, and two research vessels. Another important component of this upper-air sounding network consisted of 468 dropsondes deployed from the NOAA P3 aircraft during 12 flight missions based from Diego Garcia (DG), British Indian Ocean Territory. These dropsonde observations were intended to broaden

Corresponding author: Paul E. Ciesielski, paulc@atmos.colostate.edu

DOI: 10.1175/JAMC-D-20-0238.1

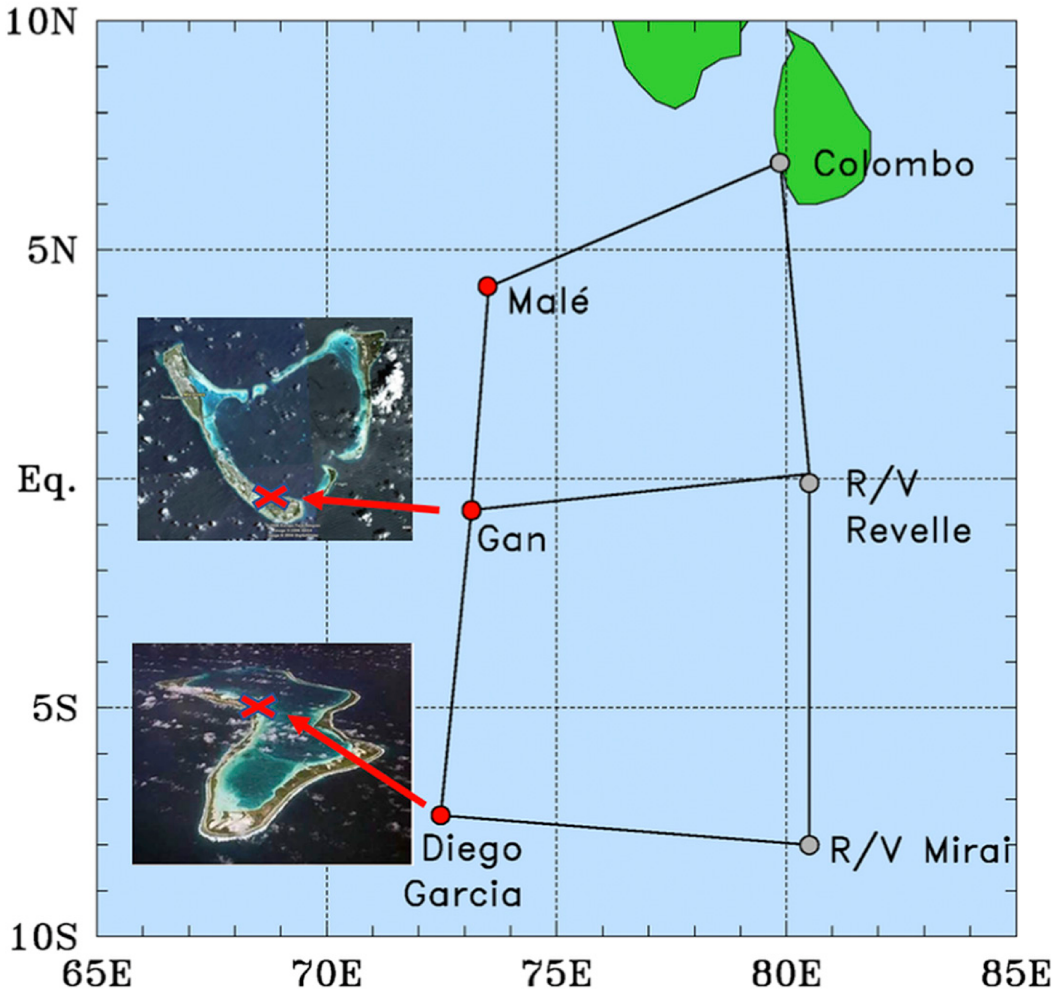

FIG. 1. Map of enhanced sounding arrays in DYNAMO. The three sites shown with red circles on the western boundary of the arrays are small islands or atolls. Insets show images from space of Addu and Diego Garcia atolls, with the red "x" denoting the approximate locations of their sounding sites.

the coverage of atmospheric measurements from the fixed locations of islands and ships by sampling the boundary layer, convective environments, and large-scale gradients of winds and thermodynamic fields. Specific details of each of the P3 missions and the processing and accuracy of dropsondes used in DYNAMO can be found in Daley (2012). Dropsonde flights in the vicinity of Gan, Maldives, and Diego Garcia during DYNAMO provide a means to examine the effects of these small atolls on the surrounding atmosphere.

In contrast to the small islands on the western edge of the sounding network, the sounding site at Colombo was located on the west coast of Sri Lanka about 100 km to the west of a north–south mountain range with peak elevations extending over 2 km. At low levels, the Colombo soundings were affected by flow blocking caused by the elevated terrain to its east and the diurnal heating of this large island. Because of the large spacing between the sounding sites in the core DYNAMO array, local island effects were aliased onto larger scales impacting analyzed fields and atmospheric budgets. To mitigate these local effects on the large-scale analyses, low-level European Centre for Medium-Range Weather Forecasts (ECMWF) operational analyses (OA) were used in a 2.5° radius around Sri Lanka to estimate open-ocean conditions at Colombo as if the island were not present (Ciesielski et al. 2014b). These open-ocean profiles were then blended with the actual Colombo soundings in the lowest 3 km of the atmosphere. During the special observing period (SOP; October and November 2011) when the sounding network was most complete (Johnson et al. 2015), the procedure resulted in a mean increase of the 925-hPa westerly flow of 2–3 $m\,s^{-1}$ in westerly regimes, a similar increase of low-level easterlies in the easterly regimes, and a muted diurnal cycle in low-level temperature and humidity more representative of oceanic conditions. In comparison with independent estimates of rainfall, use of the adjusted soundings resulted in an improved SOP-mean budget-derived rainfall and its temporal correlation over the northern sounding array (NSA) compared to

independent rainfall estimates from the Tropical Rainfall Measuring Mission (TRMM). The NSA rainfall increase due to the adjustment was ~11% of the SOP-mean (8.9 mm day^{-1}), with the largest increase of ~3 mm day^{-1} (or 38%) during a two-week period of the November MJO build-up phase. In effect, the adjusted Colombo soundings produced a beneficial impact on the NSA budgets such that the analyses better represented open-ocean conditions.

Considering the significant effect the large island of Sri Lanka had on the Colombo soundings and thereby on the DYNAMO analysis, this study considers what, if any, effect the small islands have on the surrounding atmosphere and consequently on sounding-based analyses of DYNAMO. The outline of the paper is as follows: section 2 describes the various data sources used in this study and presents a comparison of island upsondes and nearby aircraft dropsondes for a handful of cases to highlight the islands' impact on the data; the procedure to adjust the upsonde profiles to resemble atmospheric structures over the ocean is discussed in section 3 along with the impact of the adjustment on the surface data where the adjustment is the largest; section 4 considers the impact of the adjustment on large-scale analyses and convective parameters; a summary is provided in section 5.

2. Data sources and comparison of island upsondes and nearby aircraft dropsondes

a. Data

The three westernmost sounding sites in DYNAMO's enhanced sounding network (Fig. 1) were located on small island or atolls (narrow strips of land surrounding an interior lagoon). The smallest of the island sounding sites in DYNAMO, referred to here as Malé, Maldives, is actually the airport island of Hulhulé, Maldives, being roughly 4 km north–south × 2 km east–west. Sounding operations at this site were conducted less than 100 m west of the airport's main 60-m-wide north–south runway. The southernmost site, Diego Garcia, is a narrow island reef that encloses a 21 km (north–south) × 11 km (east–west) lagoon, much of which is less than 10 m deep. Sounding operations were conducted on the west side of this atoll (see inset in Fig. 1). The Gan sounding site was located near an airport runway on the southwestern end of the Addu atoll (see inset Fig. 1), which is comparable in size to that of the Diego Garcia atoll. The frequency and duration of sounding operations at each of these sites are discussed in Ciesielski et al. (2014a).

The sounding data used in this study were both from the Level 3 (L3; high vertical resolution product) as well as the Level 4 (L4) 5-hPa interpolated data. The L3 vertical resolution was 1–2 s for the upsonde sites and 0.25 s for the dropsondes. The L4 dataset has quality flags for each variable that provide a measure of the data's reliability. The three island sites, as well as the research vessels, all used Vaisala RS92 SGP radiosondes during DYNAMO. Humidity data from these sites were corrected for a daytime error referred to as the solar radiation dry bias (Vömel et al. 2007). Additional information on the quality-control procedure for these soundings, as well as all corrections applied to the various DYNAMO sites, can be found in Ciesielski et al. (2014a).

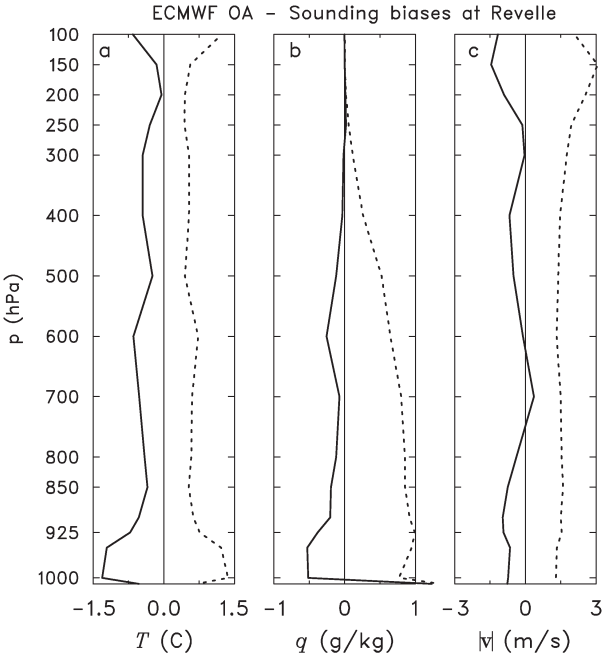

FIG. 2. Mean biases (solid) and rms differences (dashed) between ECMWF OA and soundings at R/V *Revelle* for the period from 1 Oct to 31 Dec when the ship was at nominal location 0°, 80.5°E for (a) temperature, (b) specific humidity, and (c) wind speed.

Model fields used in this study come from the ECMWF OA at 0.25° horizontal resolution, 20 vertical levels from the surface to 20 hPa, and 6-h intervals. These analyses were available for the period 1 October–31 December 2011, which coincides with the period of focus for this study. A majority (~95%) of the data from the sounding arrays were transmitted to operational centers in real time, so that the ECMWF OA in the core sounding domain are heavily influenced by the sounding data. Figure 2 shows the mean biases in temperature, specific humidity, and wind speed between the sounding data at the R/V *Revelle* (an open-ocean site) and ECMWF OA interpolated to this site. As seen at this site, there is a model cool bias throughout the troposphere peaking in the boundary, a surface moist bias that transitions rapidly to a dry bias above the surface, and a low-level negative wind speed bias. The other open-ocean sounding site, R/V *Mirai*, reveals similar biases at low-levels (not shown). The model low-level cool and dry bias and the surface moist bias are present at all the island sounding sites (not shown). The near-surface model cool bias has been attributed to excessive longwave cooling associated with the water vapor continuum in the model (Nagarajan and Aiyyer 2004). In the dropsondes Daley (2012) analyzed near DG on 4 December, a near-surface increase in moisture, referred to as a "moisture toe," was found in about 80% of dropsondes. Further analysis of the entire DYNAMO dropsonde dataset showed that 68% of drops were characterized with a moisture toe in which q increased by 0.28 g kg^{-1} over the lowest 100 m of the profile. The remaining drops had a slight decrease in moisture toward the surface such that the overall dataset average had a 0.09 g kg^{-1} increase in the lowest 100 m. The

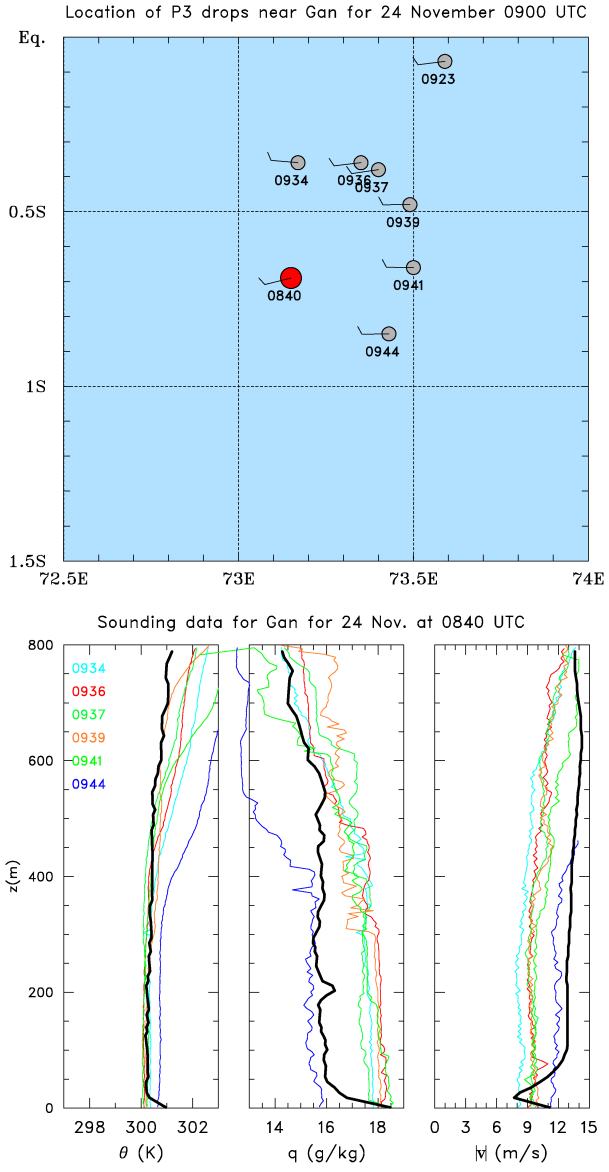

FIG. 3. (top) Location of dropsondes in the proximity of Gan (gray circles) near nominal upsonde (red circle) launch time of 0900 UTC 24 Nov (1400 LT). Wind barbs indicate wind speed (m s^{-1}) and direction at the data point closest to the surface. (bottom) Vertical profiles of (left) potential temperature θ, (center) specific humidity q, and (right) wind speed in the lowest 800 m of drops in vicinity of Gan (colored curves) and the upsonde (heavy black curves). The drop profiles are for the six drops closest to Gan, with the time of their release indicated in the bottom-left panel.

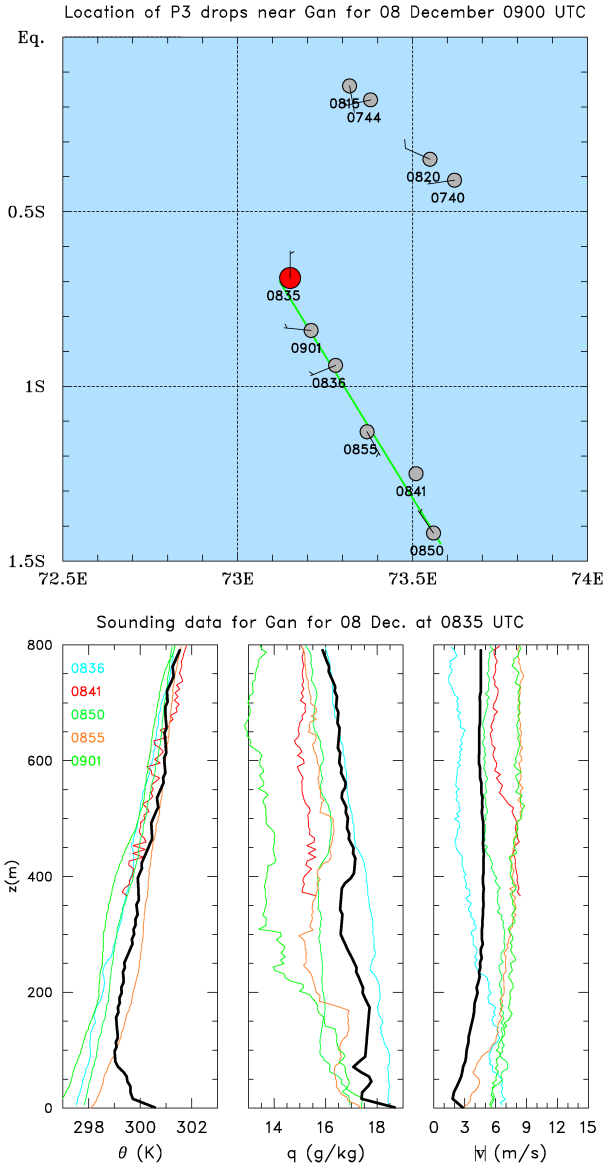

FIG. 4. As in Fig. 3, but for Gan near nominal upsonde launch time of 0900 UTC 8 Dec (1400 LT). The drop profiles are for five drops southeast of Gan along the green line shown in the top panel.

presence of this near-surface q gradient and the fact that the ECMWF q field is provided at 2 m while the *Revelle* surface data are given at 19 m likely contributes to, but cannot fully account for, the much larger surface moisture bias seen in Fig. 2. The model surface wind speed bias at the island sites (not shown) is positive reflecting the frictional effect of the islands on the near-surface sounding winds. This positive bias is 0.2 m s^{-1} at Malé, 1.3 m s^{-1} at Gan, and 2.3 m s^{-1} at Diego Garcia. The differences in the wind speed bias among the sites likely reflect the differences in the size of the islands as well as where the radiosondes were launched with respect to the island's configuration. In short, using the ECWMF OA as was done at Colombo[1] is not a viable option here, as it would introduce the model biases into adjusted soundings. The model biases seen in Fig. 2 will serve as a benchmark for open-ocean sounding biases.

[1] ECMWF OA model biases were considerably smaller in the vicinity of Colombo as shown in Fig. 4 of Ciesielski et al. (2014b).

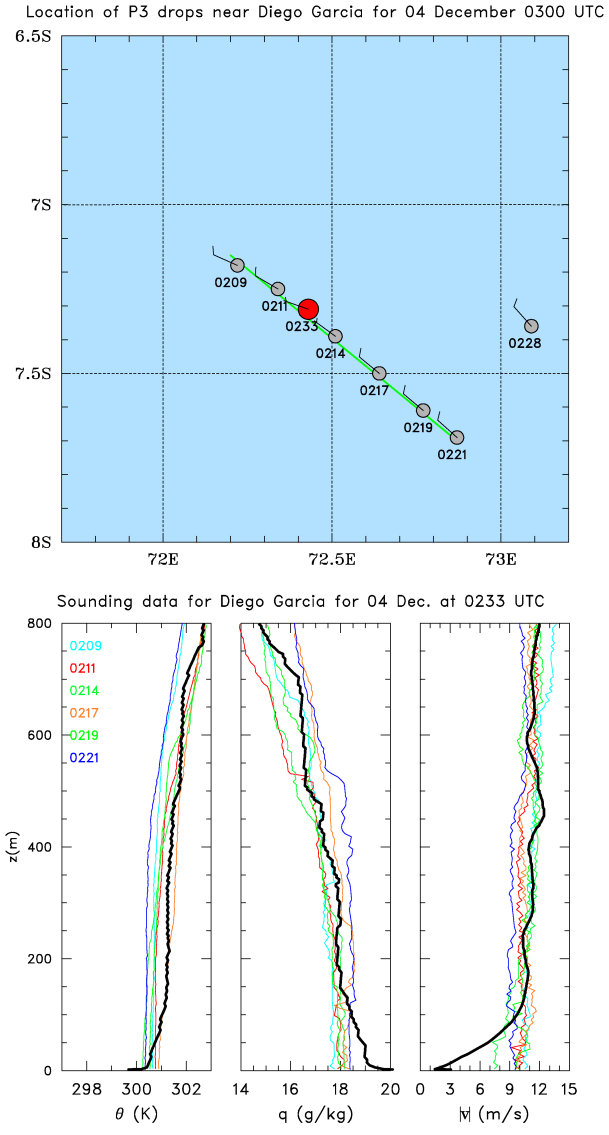

FIG. 5. As in Fig. 3, but for DG near nominal upsonde launch time of 0300 UTC 4 Dec (0800 LT). The green line in the top panel represents the location of the cross section shown later in Fig. 6. The drop profiles are for six drops along that green line.

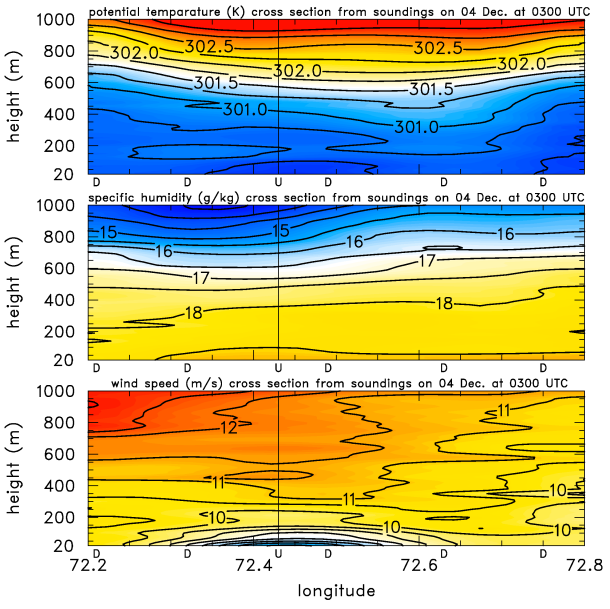

FIG. 6. Height cross section along the line shown in the top panel of Fig. 5 constructed using the dropsonde and upsonde data shown in the bottom panels of Fig. 5 for 0300 UTC 4 Dec (0800 LT), showing contour plots for (top) θ, (middle) q, and (bottom) wind speed. The vertical line indicates the island upsonde location, and "D" symbols along the bottom axes show the locations of dropsondes. Analyses are not shown below 20 m because data for some dropsondes are missing below this level, making it difficult to analyze.

Other data sources used in this study include rainfall analyses available at 3 h and 0.25° horizontal resolution available from the 3B42v7 TRMM product (Huffman et al. 2007). For computation of budget-derived rainfall as a residual from the moisture budget (Yanai et al. 1973), surface latent heat fluxes were obtained from the TropFlux product (daily, 1° horizontal resolution) based on Praveen Kumar et al. (2012).

b. Island effects as depicted in upsonde and dropsonde data

Of the 468 dropsondes deployed in DYNAMO, 39 were taken within 100 km of Gan and 50 within 100 km of Diego Garcia, allowing us to examine the magnitude and scope of influence these island/atolls have on their surrounding atmosphere. In addition, comparison of the island upsondes with nearby dropsondes over the ocean helps to better quantify the islands' impacts on the upsonde observations. There were 4 flights with multiple drops in vicinity of Gan and 13 such flights in the vicinity of Diego Garcia. In the interest of space, we consider only a few cases for each site to illustrate how the islands modify their marine environment. While the dropsondes in DYNAMO were typically released between 3 and 5 km, providing data from these altitudes to the surface, results below are shown in the lowest 800–1000 m of the atmosphere to emphasize the island effects.

Figure 3 (top panel) shows a map with the location of dropsondes in the vicinity of Gan Island on 24 November near the time of the 0900 UTC (1400 LT) upsonde launch. The bottom panel of this figure shows the L3 (high vertical resolution) profiles of potential temperature θ, specific humidity q, and wind speed $|\mathbf{v}|$ for the dropsonde and upsonde data for this case. The times of the dropsondes, shown in these figures, were all about an hour after the upsonde launch. Well-mixed boundary layers of various depths are present in most of these profiles along with wind speeds ranging from 10 to 15 m s^{-1}. There is no obvious evidence of the island effects in the drops that are all 30 km or farther from Gan. On the other hand, island effects in the upsonde are seen as slight surface warming (~1°C) below 30 m, a moistening below 50 m peaking at 2 g kg^{-1} near the surface, and a wind speed reduction from 13 m s^{-1} at 100 m to 8 m s^{-1} at 20 m. The low-level westerlies in this case would have taken the radiosonde over the atoll lagoon that may account for the low-level surface moisture increase.

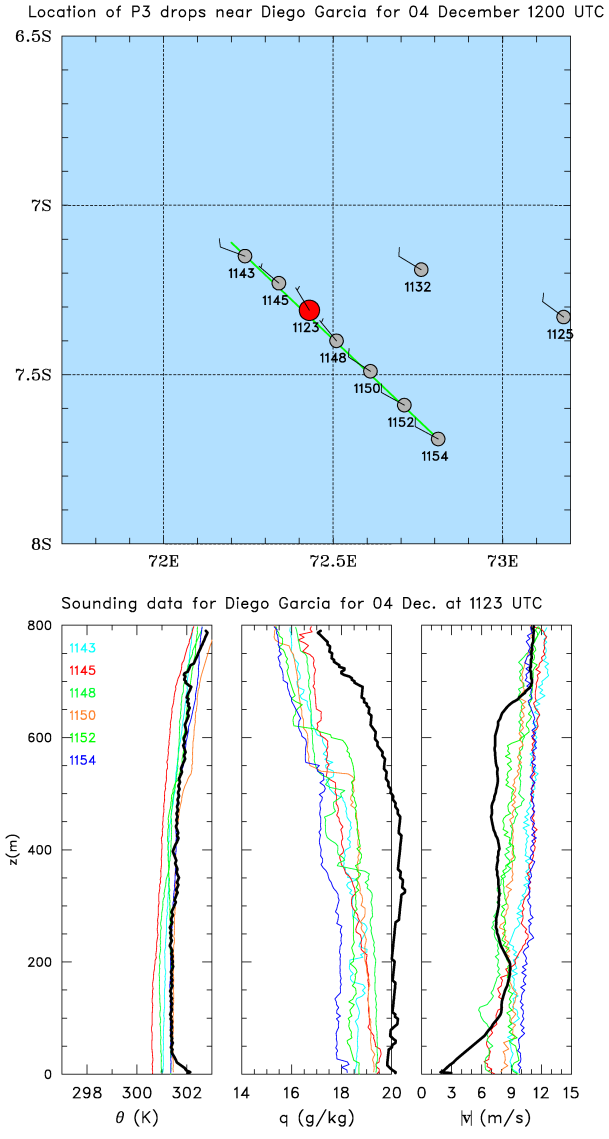

FIG. 7. As in Fig. 3, but for DG near nominal upsonde launch time of 1200 UTC 4 Dec (1700 LT). The green line in the top panel represents the location of the cross section shown later in Fig. 8. The drop profiles are for six drops along that green line.

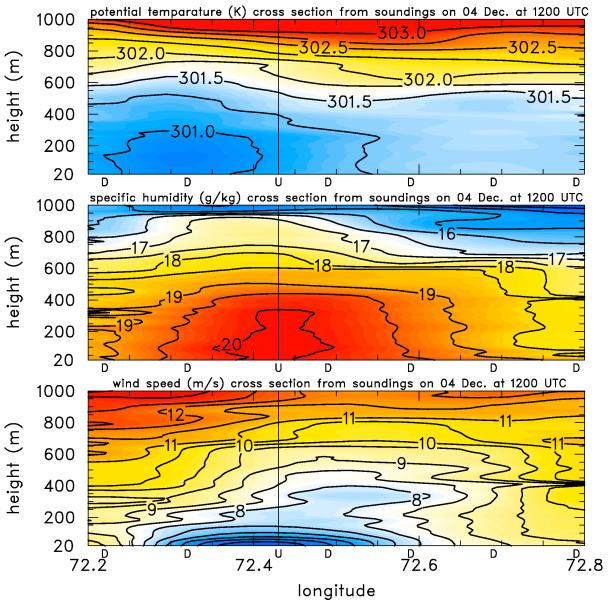

FIG. 8. As in Fig. 6, but for the height cross section along the line shown in the top panel of Fig. 7 constructed using the dropsonde and upsonde data shown in the bottom panels of Fig. 7 for 1200 UTC 4 Dec (1700 LT).

The next case considered for Gan (Fig. 4) on 8 December near 0900 UTC (1400 LT), was characterized with lighter winds (ranging from 2 to 8 m s^{-1}) and stable conditions with potential temperature increasing with height in all the drop profiles. Again, there are no obvious island effects in any of the drops. Even though the drop at 0901 UTC is within 16 km, it is not downwind of the island due to its location south-southeast of the island and the presence of low-level westerlies at this time. The island effects in the Gan sounding include a temperature increase most obvious below 80 m with a 2°C increase near the surface over the drops, a moisture increase of 1 g kg^{-1} below 20 m, and a wind speed reduction of 2–3 m s^{-1} below 200 m. The lighter winds during this time may account for the larger near-surface warming compared to the earlier case. The moisture variability is quite large among the various profiles reflecting the large mesoscale spatial variability in moisture at this time, possibly indicating the presence of significant mesoscale variability owing to boundary layer (Weckwerth et al. 1999) and/or local island-induced (Wang and Sobel 2017) circulations.

With the P3 operations being based from DG, there were 13 cases of near-contemporaneous drops and island launches to consider. In what follows, 3 cases are presented that had good data coverage of drops in the vicinity of DG and represent a range of environmental conditions. On 4 December, two missions were flown in the vicinity of DG (one around 0800 LT and a second around 1600 LT) specifically to sample the boundary layer in the vicinity of the atoll and its evolution from morning to late afternoon. The synoptic conditions over the region were dominated by mostly clear skies and persistent northwest flow greater than 10 m s^{-1} at low levels (Daley 2012). The location of the drops and the sounding profiles for the morning mission are shown in Fig. 5. In this case and the evening flight, the drops were made along a northwest–southeast line over the island and along the wind shear vector in order to examine the upstream and downstream impacts of DG on the environment. As seen in the bottom panel of Fig. 5, the island effects on the DG sounding are a 1°C near-surface reduction in temperature, a 1 g kg^{-1} near-surface increase in moisture, and a wind speed reduction below 100 m peaking near the surface at ~10 m s^{-1}. To better depict the island impacts on atmosphere sampled by the dropsondes, Fig. 6 shows a vertical cross section (from 20 m to 1 km) of the fields along the line of the drops. As seen here, the near-surface cooling extends downwind about 10 km, the enhanced near-surface moistening appears both upstream and downstream about 10 km, while the low-level wind speed reduction is seen both upstream ~15 km and up to 20 km downstream of DG.

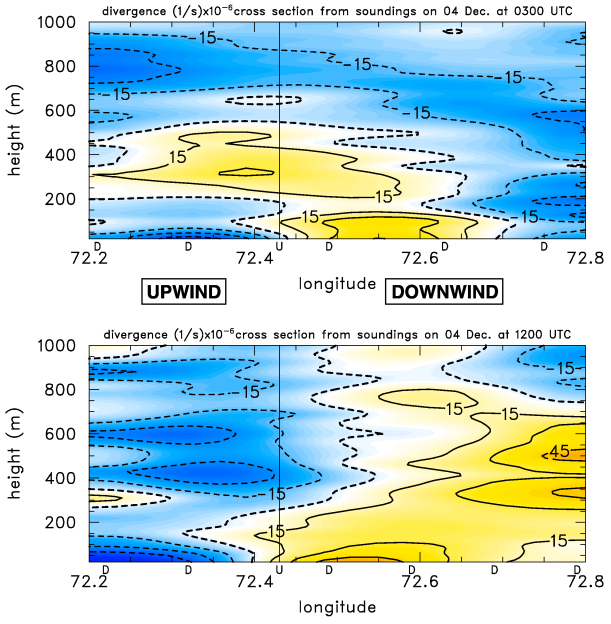

FIG. 9. Height cross section of divergence near DG based on (top) morning 0300 UTC (0800 LT) and (bottom) evening 1200 UTC (1700 LT) observations on 4 Dec. Blue and yellow shadings represent areas of convergence and divergence, respectively. The vertical line shows the island upsonde location such that areas to the left of the line represent upwind conditions and areas to the right of the line represent downwind conditions; the "D" symbols along the bottom axes show the locations of dropsondes.

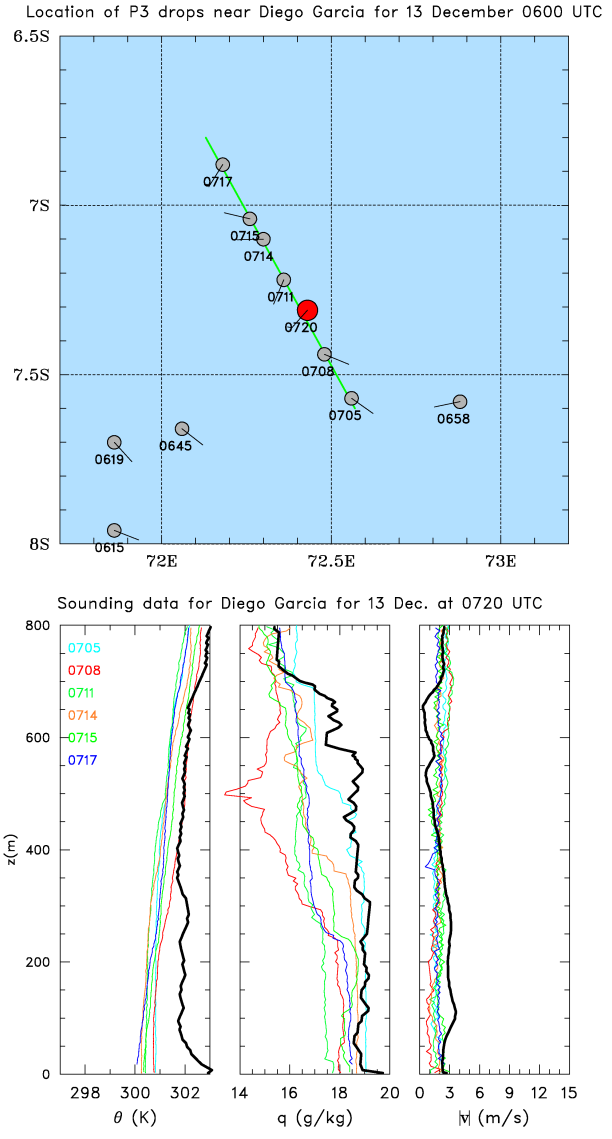

FIG. 10. As in Fig. 3, but for DG near the time of 13 Dec 0700 UTC (1200 LT). The drop profiles are for those along the green line shown in the top panel.

These island effects have little vertical depth (<100 m) and are centered slightly downstream of the upsonde launch site.

The island impacts on the surrounding atmosphere are more pronounced in the late afternoon soundings. Similar to the morning flight, the late afternoon mission provided two upwind and four downwind drops in a northwest–southeast line over DG (Fig. 7). The island effects on the DG sounding are seen as a 1°C near-surface warming, a deep enhanced moistening of 1–2 g kg^{-1}, and wind speed reduction of ~6 m s^{-1} below 100 m. The island impacts viewed in a vertical cross of the fields (Fig. 8) show a 500-m deep moist pocket of air centered over DG extending both 20–30 km both upstream and downstream from the island, and a low-level wind reduction evident ~20 km upstream and nearly 45 km downstream of DG. It is also noteworthy that the layer of reduced wind speeds deepened vertically from ~200 m upwind to about 600 m downwind of the island. The enhanced late afternoon impact of the island on the moisture field is likely related to diurnal heating of the atoll's shallow lagoon (maximum depth is 25 m with about half the lagoon being less than 10 m deep). On this clear-sky day, solar heating of the lagoon likely resulted in high afternoon SSTs, promoting strong latent and sensible heat fluxes and thus enhanced moisture and heat plumes, respectively, contributing to the moist, deep boundary layer at this time.

The location of drops on 4 December, being along the shear vector, make it possible to capture the low-level divergence structure in this plane as shown in Fig. 9 for the morning and evening drops. Upwind of DG near-surface convergence is present at both times with low-level divergence downwind. This low-level divergence pattern, which strengthens in the afternoon analysis (bottom panel), results from the reduction in wind speed over the island due its increase in surface friction. For the wind speeds present in the vicinity of DG on 4 December (10–15 m s^{-1}), the numerical simulations in Wang and Sobel (2017) showed strong asymmetries in rainfall between the upwind and downwind sides of the island with enhanced (reduced) rainfall on the windward (lee) side. They attribute this rainfall pattern to gravity waves resulting from the land–sea contrast in surface roughness along with an upward deflection of the horizontal flow by elevated diurnal heating. Though convective conditions

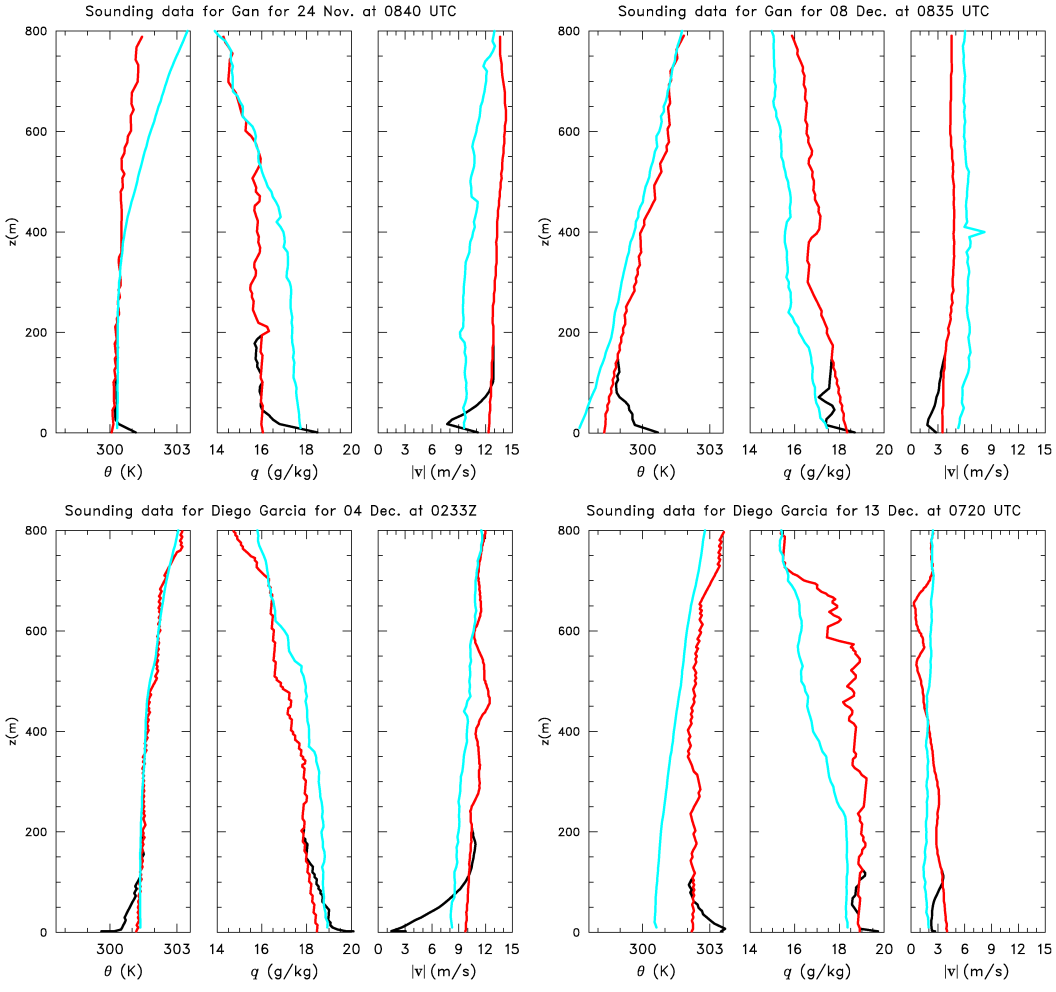

FIG. 11. Vertical profiles (in each three-panel set) of θ, q, and wind speed for unadjusted (black) and adjusted (red) upsonde data and average proximity dropsonde data (cyan). Profiles are shown for (left) strong wind and (right) weak wind situations at (top) Gan and (bottom) DG taken from cases discussed earlier.

near DG were generally suppressed on 4 December, the low-level divergence pattern and implied vertical motion field are consistent with the asymmetric rainfall pattern described above.

In contrast to the strong wind cases, the light-wind case on 13 December 0700 UTC (1200 LT) shows a much deeper impact on temperature (Fig. 10). At this time, the active phase of the MJO was over the Maritime Continent, with suppressed conditions present over much of the DYNAMO domain and clear skies with light wind conditions prevailing over DG. Here the near noontime island sounding shows an ~3°C increase in near-surface temperature relative to the nearby drops. This temperature increase is largest in the lowest 100 m but extends to nearly 350 m. A near-surface (lowest 20 m) moistening (~1 g kg^{-1}) is present in the island sounding that is not seen in any of the nearby drops. Interestingly, the moisture profile of the island sounding is very similar to the dropsonde profiles at 0705 and 0714 UTC that are 33 and 25 km away, respectively. However, the nearest drops to the island at 0708 UTC (17 km) and 0711 UTC (11 km) are 1–2 g kg^{-1} drier from the surface to ~700 m. This might suggest that the heating of the atoll/lagoon complex has produced a local sea-breeze circulation with the drier profiles evidence for the subsiding branches of the cell.

3. Adjustment procedure

Figure 11 shows the vertical profiles of potential temperature, specific humidity, and wind speed for four of the cases described in previous section, where the nearby dropsonde profiles have been

TABLE 1. Definition of averaging layer as a function of the mixed-layer top z_i. In adjustment procedure, this layer is used for computing the average vertical gradient of a field. The last column shows the fraction of soundings in each category.

z_i	Averaging layer	Percent of soundings
>400 m	z_i–200 m	49.0
250–400 m	From z_i to z_i − 200 m	12.4
<250 m	z_i–50 m	4.5
Not defined	500–200 m	34.1

TABLE 2. Mixed-layer statistics for three island/atoll sites in DYNAMO. Mean rainfall rate and frequency are computed from 3-h TRMM 3B42 data.

Site	Period	Mean z_i (m)	z_i frequency	Mean rainfall (mm day^{-1})	Rainfall frequency
Malé	1 Oct–15 Dec	535	71.5%	5.6	53%
Gan	1 Oct–31 Dec	503	67.1%	7.5	62%
Diego Garcia	1 Oct–31 Dec	495	66.5%	8.7	71%

averaged together. In each case the mean dropsonde profiles (cyan curves) show a generally constant gradient over the lowest 500 m of the profile, while the island effect on the upsonde data (black curves) is clearly evident with rapidly changing gradients in the lowest few hundred meters. Based on this observation that vertical gradients of θ, q, and wind speeds over the open ocean are generally constant in the lowest 0.5 km of dropsondes (apart from disturbed conditions such as precipitation downdraft outflows), a simple procedure was constructed to adjust the upsonde profiles in the lowest few hundred meters to resemble the atmospheric structures over the ocean. The procedure employed here was patterned after that used by Yoneyama et al. (2002) to correct ship soundings for deck heating and cooling effects that were observed in the lowest 40 m at the R/V *Mirai*. In their procedure they linearly extrapolated good data in the sounding down from 50 m to the surface. Since comparison of island soundings with nearby dropsondes shows that islands' impact was most prominent in the lowest 200 m of the sounding profile, we limit our procedure to this layer.

As seen in the cases examined above, island impacts extended above 200 m in some soundings. To estimate of the percent of island radiosondes with impacts deeper than 200 m, simulated open-ocean soundings were created for the island sites by 1) sampling the ECMWF OA fields in a 1° radius around the island sounding sites, 2) objectively analyzing these large-scale fields to the sounding location, and 3) subtracting the open-ocean ECMWF mean bias for each field as depicted for the R/V *Revelle* in Fig. 2. The island's impact at a given level is then estimated as percent of time that the simulated open-ocean sounding differs from the actual island sounding by more than the rms difference shown in Fig. 2. At 950 hPa (~535 m, i.e., a deeper island impact), this percentage averaged over the three island sites is ~2%, 30%, and 31% for T, q, and $|\mathbf{v}|$, respectively, where the rms differences for these fields at this level are 1.2°C, 1.0 g kg^{-1}, and 1.3 m s^{-1}, respectively. The percentages differ slightly among the sites, being smallest for Malé and largest for DG (not shown). The small percentage for T is likely related to the weak T gradients observed in the tropics, while the higher percentages for the other fields reflect their high spatial and temporal variability due to mesoscale circulations and island effects. While this crude estimate suggests that deeper island impacts may be significant up to 30% of the time, these deeper effects are difficult to identify without additional data sources, and thus are difficult to remove with an objective procedure, and hence are not addressed further in this study.

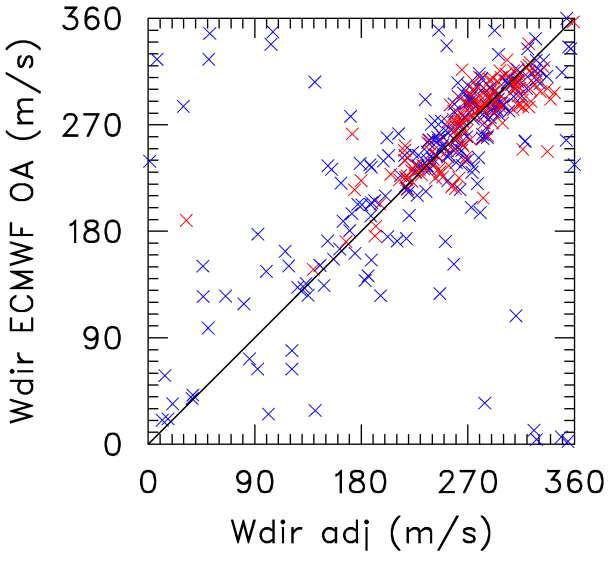

FIG. 12. Scatterplot for wind direction (Wdir) at Gan with ECMWF values plotted along the y axis and gradient-adjusted values plotted along x axis. Values that are less than the period-mean wind speed (5.0 m s^{-1}) are plotted in blue, and values that are greater than the period mean are plotted in red.

Our procedure for mitigating the effects of the small islands in DYNAMO on the upsonde data is as follows: 1) In the cases in which a mixed layer was present, the average gradient of winds, temperature, and moisture was computed within this layer using the 5-hPa resolution L4 data.[2] Depending on the height of the mixed-layer top z_i, several different averaging procedures were adopted as listed in Table 1. Better results were achieved with deeper averaging layers, which motivated the design of these different averaging scenarios. Note from this table that 95% of the soundings had an averaging layer at least 200 m deep. 2) If no mixed layer was present, the average gradient of these fields was computed from 500 to 200 m, the 500-m height being the approximate average level of z_i at the island sites (Johnson and Ciesielski 2017) in the DYNAMO domain. 3) These average gradients were then used to compute the adjusted winds, T, and q fields by extrapolating these gradients from the bottom of the averaging layer (i.e., 200 m unless $z_i < 400$ m) to the surface. Gradients for the u and v wind components were computed separately with adjustments made to the wind components. These components were then used to compute an adjusted wind speed and direction. 4) After applying this procedure, all adjusted soundings were visually

[2] The advantage of using the L4 dataset is that its quality flags allow us to easily use only good data for computing gradients.

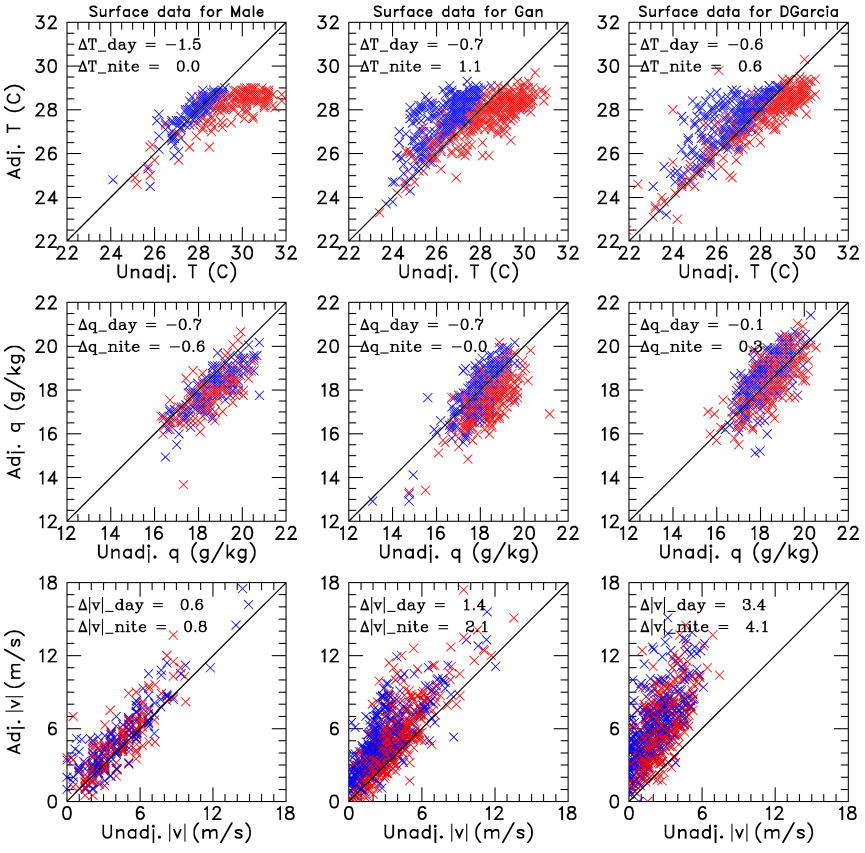

FIG. 13. (top) Scatterplots for adjusted vs unadjusted surface (top) temperature T, (middle) q, and (bottom) wind speed $|\mathbf{v}|$ data for (left) Malé, (center) Gan, and (right) DG. Red symbols are for daytime soundings, and blue symbols for nighttime soundings. Values listed in the panels represent mean daytime and nighttime changes due to adjustments (i.e., adjusted minus unadjusted values).

inspected to ensure a reasonable adjustment. In ~8% of the soundings, unrealistically large surface adjustments (>1 standard deviation from the mean surface value) resulted from the computed average gradient differing substantially from the vertical gradient in the lower part (50–100 m) of the averaging layer. In these cases, the averaging layer was adjusted slightly to improve the low-level adjustments.

An important aspect of the above procedure is having an accurate determination of the presence of a mixed layer and its depth. This is done subjectively using the L4 5-hPa sounding data where a sounding is identified as having a mixed layer if the following conditions are met: θ is approximately constant with height from the surface (or the top of a superadiabatic layer when it exists) up to a height z_i, the mixed-layer top, with an abrupt increase in stability above z_i, and q is constant or decreases only slightly from the surface up to z_i and then decreases rapidly above. Additional details of this identification procedure can be found in Johnson and Ciesielski (2017), which provides z_i estimates for sites in the NSA of DYNAMO. To complete these estimates for all of the small island sites in DYNAMO, this procedure was applied to soundings from Diego Garcia. Table 2 summarizes some key mixed-layer statistics for these island sites for the period over which their soundings were used in this study. As noted in Johnson et al. (2001) the mean mixed-layer depth is often related to rainfall rates and frequency such that shallower mean z_i occurs with greater rainfall rates and frequencies, implying a higher frequency of recovering precipitation downdraft wakes. This relationship holds true for the mixed-layer statistics presented in Table 2 with Diego Garcia having the shallowest mean z_i and the greatest and most frequent rainfall.

TABLE 3. Frequency of surface nighttime inversions and surface daytime superadiabatic layers for soundings launched during the period from 1 Oct to 31 Dec 2011.

Site	No. of radiosondes	Frequency of nighttime inversions	Frequency of daytime superadiabatic layers
Malé	318	8.5%	5.3%
Gan	714	45.7%	1.3%
Diego Garcia	616	26.3%	1.0%
R/V *Revelle*	514	0.8%	0.8%
R/V *Mirai*	483	0.0%	0.0%

TABLE 4. ECMWF OA − radiosonde biases using unadjusted (in parentheses) and adjusted surface data for the period from 1 Oct to 31 Dec 2011 separated for day (0800, 1100, 1400, and 1700 LT) and night (0200, 0500, 2000, and 2300 LT). ECMWF values represent data at 1° radius interpolated to site locations. Values at the *Revelle* and *Mirai* are included here to represent model bias for open-ocean conditions.

Surface field	Malé	Gan	DG	*Revelle*	*Mirai*
T_day (°C)	(−1.0) 0.5	(−0.6) 0.1	(−1.2) −0.6	−0.6	0.2
T_night (°C)	(−0.7) −0.7	(0.3) −0.8	(−0.4) −0.9	−0.4	0.4
q_day (g kg^{-1})	(0.7) 1.4	(0.7) 1.4	(−0.1) 0.0	2.0	1.7
q_night (g kg^{-1})	(0.0) 0.6	(0.7) 0.7	(0.0) −0.3	1.1	1.6
$\|\mathbf{v}\|$_day (m s^{-1})	(−0.3) −1.0	(0.7) −0.7	(2.2) −1.2	−0.8	−0.9
$\|\mathbf{v}\|$_night (m s^{-1})	(0.0) −0.8	(1.5) −0.7	(2.9) −1.2	−0.7	−1.2

Figure 12 shows a scatterplot of the gradient-adjusted (GA) surface wind direction at Gan versus that from the ECMWF OA interpolated to the Gan location. As seen here much of the scatter from the one-to-one line is for light wind situations in which the island sounding may be sampling local circulations not representative of the large-scale open-ocean flows represented in the model analysis. Plots for the other island sites (not shown) exhibit similar characteristics. To account for this concern, a second adjustment step was applied to the sounding wind field using the following procedure: 1) sample the ECMWF OA winds in a 1° radius around the island sounding site, 2) objectively analyze this large-scale model wind field to the sounding location, 3) then blend the model and GA winds such that the resulting wind direction smoothly transitions

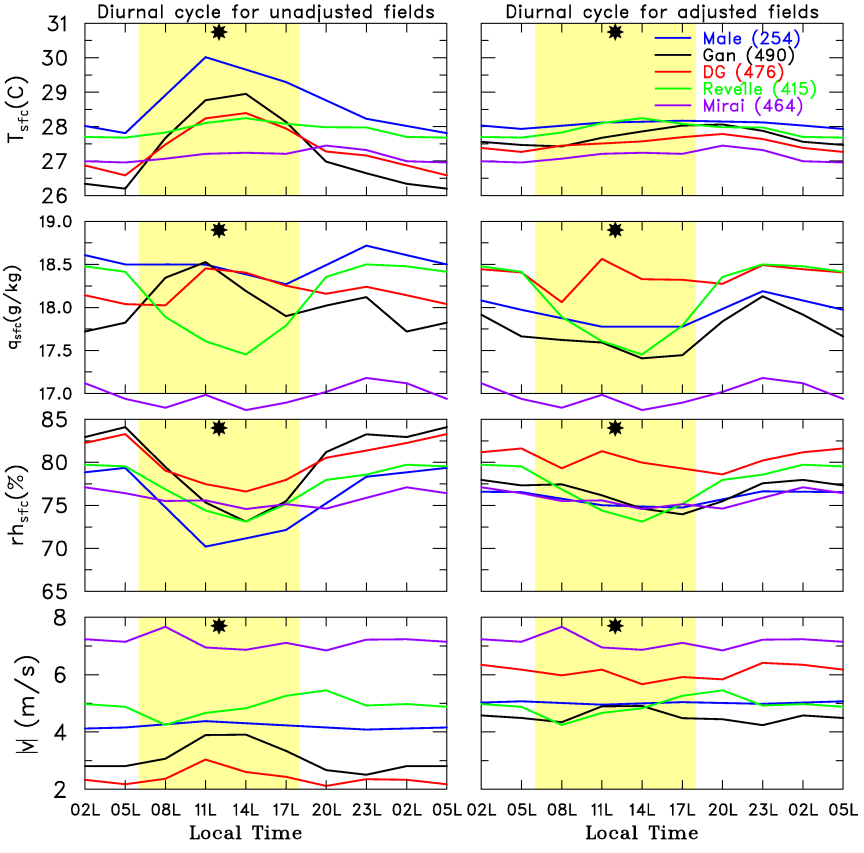

FIG. 14. Diurnal cycle of the (left) unadjusted and (right) adjusted surface fields from 1 Oct to 30 Nov 2011 for (top) T, (top middle) q, (bottom middle) relative humidity rh, and (bottom) $|\mathbf{v}|$. Results are shown for Malé (blue), Gan (black), DG (red), and open-ocean sites *Revelle* (green) and *Mirai* (purple). Numbers in paratheses indicate the number of soundings used. Daytime hours are highlighted in yellow, and asterisks denote local noon.

from 100% GA winds at 200 m to 100% model winds at the surface.[3] This blending approach is similar to that used in Ciesielski et al. (2014b) [see their Eq. (1)]. A 1° radius was chosen for sampling the model winds, that being a scale small enough to yield a realistic representation of the flow field in the vicinity of the islands but large enough to avoid any possible island effects.

The adjustment procedure described above was applied to all soundings at Malé, Gan, and DG for the period 1 October–31 December. Figure 11 shows the profiles for the unadjusted (black curves) and adjusted sounding fields (red curves) for four of the cases considered in section 2. As seen for these cases, the low-level gradients in the adjusted island radiosonde profiles appear to capture similar gradients in the mean dropsonde profiles, such that the procedure appears to effectively eliminate the low-level island impacts on the soundings.

To assess the reasonableness of the adjustments we now consider some of their general characteristics, focusing on their effect on surface fields where the adjustments are typically largest. Scatterplots of surface temperature with and without adjustments are shown in Fig. 13 (top panel) for the three island sites. The overall mean adjustment, separated for day (red) and night (blue) radiosondes, is listed for each site. From this we note that in the mean the adjustment acts to cool the daytime temperatures and warm the nighttime temperatures. This seems reasonable as heating and cooling at the island's surface would result in nighttime stable layers and daytime superadiabatic layers. This adjustment effectively removes these island-induced surface features.

The surface temperature adjustments, which vary from site to site, are likely related to the size of each island and where the radiosondes are launched. For example, Malé has the largest mean daytime correction (−1.5°C) and a near zero mean nighttime correction. The radiosondes at this site were launched near, and west of, a large runway that likely contributed to daytime surface heating sensed by the radiosonde, whereas the island's small size and proximity to the runway may have inhibited nighttime surface cooling. The frequencies of nighttime surface inversions and daytime superadiabatic layers are 8.4% and 7.5% at Malé, respectively, which are very different from these occurrence rates at the other island sites (>25% and ~1%); see Table 3 for these rates at all sites. The procedure effectively removes these island-induced surface features with occurrence rates at or near zero in the adjusted radiosondes similar to what is observed at the *Revelle* and *Mirai*. The mean nighttime adjustment is largest at Gan (+1.1°C), which is consistent with the highest rate of nighttime inversions in the unadjusted data.

Scatterplots of the surface moisture and wind speed with and without adjustments are also shown in Fig. 13 (middle and bottom panels) for the three island sites. As seen here, the adjustments at the surface produce a drying at Malé both day and night, a drying at Gan during the day, with little mean adjustment at Gan during the night and at DG. The surface wind speed adjustment is nearly always positive (90% of time) and slightly larger at night, which is consistent with the idea that reduced mixing associated with island-induced stable layers results in weaker nighttime winds. The wind speed adjustment is smallest at Malé, which one might expect with it being the smallest island.

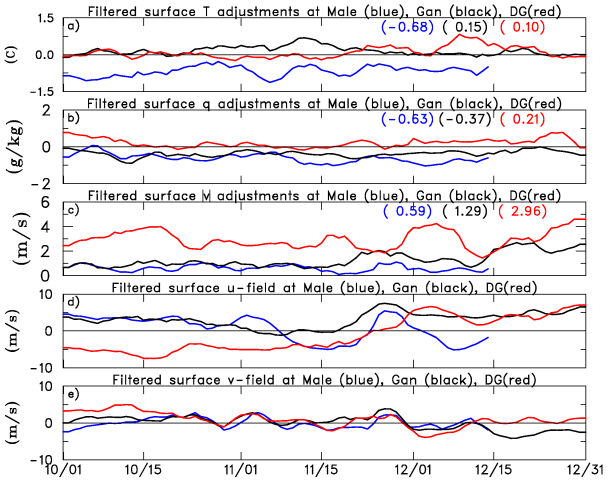

FIG. 15. Time series of filtered (5-day running average of daily means) changes (adjusted minus unadjusted) in gridded analyses averaged over a 1°-radius area centered on Malé (blue), Gan (black), and DG (red) for (a) T, (b) q, (c) $|\mathbf{v}|$, (d) u, and (e) v. The numbers in parentheses show the period means.

A list of ECMWF OA model biases versus unadjusted and adjusted surface sounding data is given in Table 4 along with the model biases at the ships that serve as an open-ocean benchmark for these comparisons. To mitigate local island effects in the model data, model variables at a 1° radius surrounding the sounding sites were interpolated to the sounding locations. At the ships, the model surface winds are ~1 m s^{-1} weaker than the sounding winds. Despite the differences in the speed adjustments at the island sites (0.7 m s^{-1} at Malé, 1.7 m s^{-1} at Gan, and 3.7 m s^{-1} at DG), the mean speed bias (model minus adjusted soundings) at these sites is very similar to that of the open-ocean sites lending credibility to the adjustment. In general, the model biases of the adjusted values at the island sites span the range of biases found at the open-ocean sites. The notable exception to this is the adjusted surface moisture bias at DG where instead of a model moist bias seen at the other sites, little, if any, model bias is seen.

To further examine the adjustments, Fig. 14 shows the diurnal cycle of the unadjusted and adjusted surface fields for the DYNAMO SOP when data coverage for these sites was most complete. The diurnal cycle of surface fields from the *Mirai*'s and *Revelle*'s sounding data is included as a benchmark for open-ocean conditions. The amplitude of the surface temperature diurnal cycle at island sites is ~2.5°C in the unadjusted

[3] Since variations in z_i (i.e., mixing depth) were considered in the gradient adjustment, for simplicity, the blending of the model and GA winds was confined to a constant layer (i.e., the lowest 200 m of each radiosonde profile).

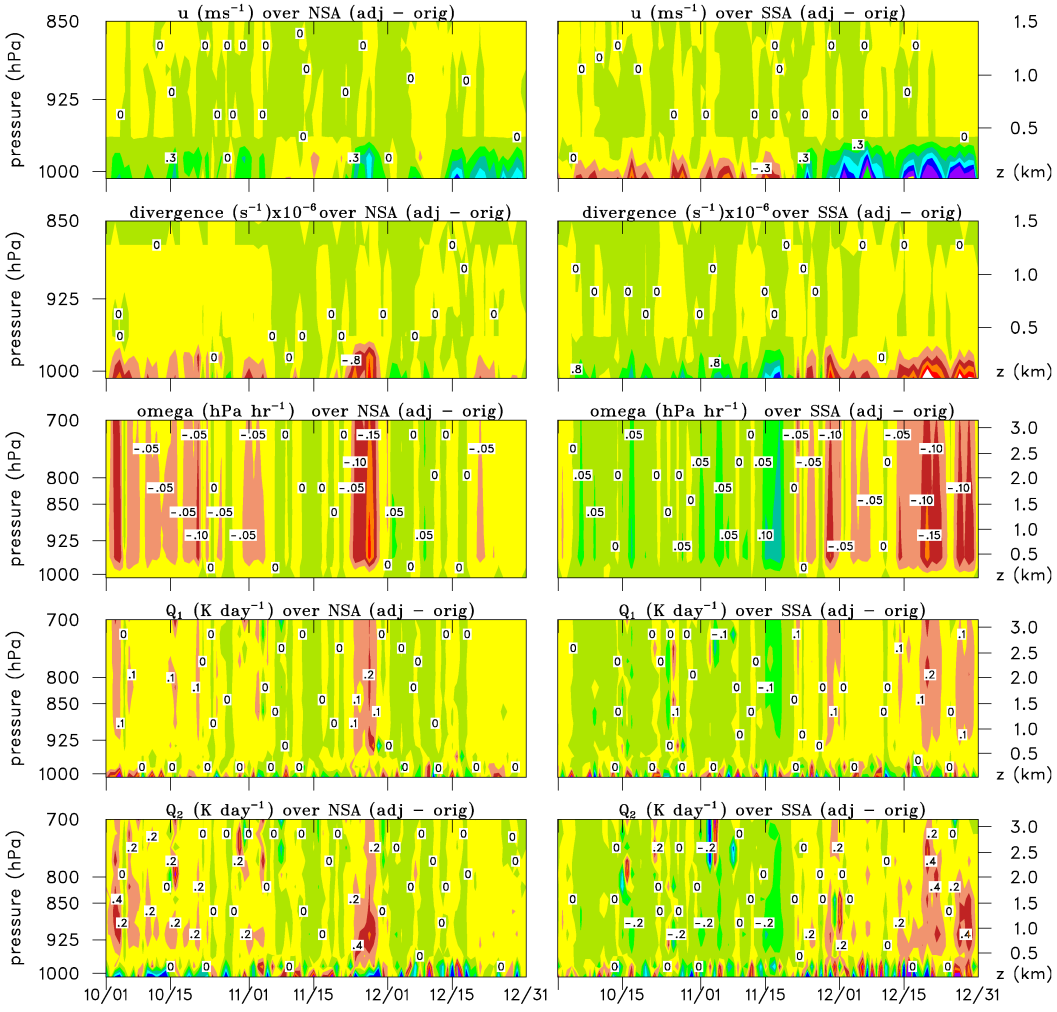

FIG. 16. Time–height plots of change due to adjustments in (top) zonal wind, (top middle) divergence, (middle) vertical motion, (bottom middle) Q_1, and (bottom) Q_2 averaged over (left) NSA and (right) SSA (with contour intervals 0.3 m s^{-1}, 0.8 × 10^{-6} s^{-1}, 0.05 hPa h^{-1}, 0.01 K day^{-1}, and 0.02 K day^{-1}, respectively). Note the different vertical ranges in the top two panels (from the surface to 850 hPa) as opposed to the bottom three panels (from the surface to 700 hPa).

data, whereas in the adjusted data its amplitude is similar to that observed at the ships, that is, ~0.5°C. For surface moisture, the specific humidity peaks during the day at Gan and DG in the unadjusted fields but at night in the adjusted fields similar to the ships. The diurnal amplitude of relative humidity (rh) is ~10% in the island unadjusted data but ~3% using the adjusted data. The rh diurnal cycle amplitude is 6.5% at the *Revelle* and 2.5% at the *Mirai* that bracket the island-adjusted values. The surface wind speeds at the ships exhibit no systematic diurnal cycle, whereas Gan and DG show daytime peaks and nighttime minima in the unadjusted speeds. The preponderance of nighttime stable layers at these sites (see Table 3) would inhibit vertical mixing resulting in reduced nighttime speeds. However, the speed adjustment is larger for the nighttime radiosondes (Fig. 13) such that the adjusted speeds show little diurnal cycle similar to the ships. The magnitudes of the adjusted speeds at Malé and Gan are similar to those at the *Revelle*, while the speeds at DG are bracketed by the two open-ocean sites. In summary, the diurnal cycle characteristics of the adjusted surface data are consistent with open-ocean sites, giving us confidence that our procedure has produced desired results.

4. Impact of adjustments on large-scale budgets and convective parameters

For the analyses in this section, gridded fields of the horizontal wind components, temperature, water vapor mixing ratio, and geopotential height were produced at 3-h intervals, 1° horizontal resolution, and 25-hPa vertical resolution from 1000 to 25 hPa using multiquadric interpolation (Nuss and Titley 1994) with details described in Johnson et al. (2015).

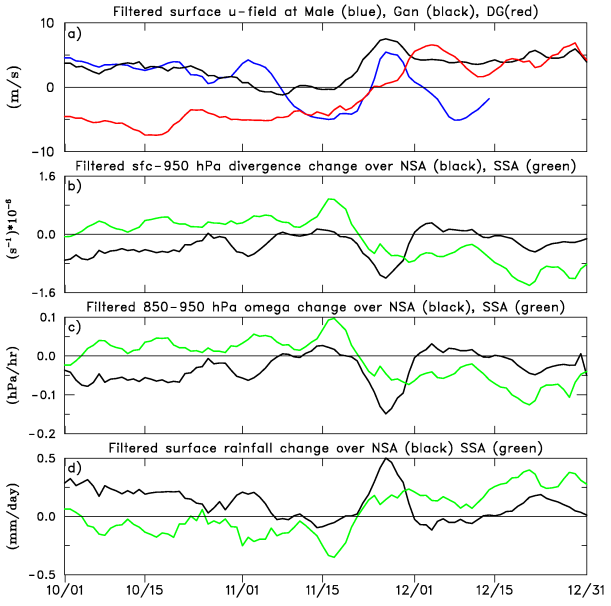

FIG. 17. Time series of filtered (5-day running average of daily means) surface fields: (a) wind at Malé (blue), Gan (black), and DG (red) and (b) divergence from the surface to 950 hPa, (c) 950–850-hPa vertical motion, and (d) Q_2 budget–derived rainfall for NSA (black) and SSA (green).

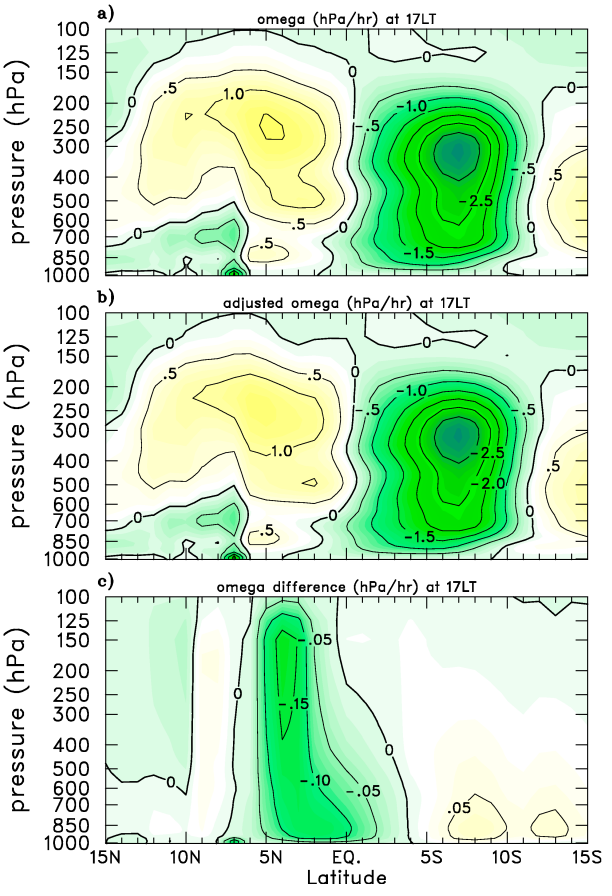

FIG. 18. Latitude–height cross section averaged over 72°–80°E of omega computed using (a) unadjusted soundings and (b) adjusted soundings and (c) their difference (adjusted minus unadjusted) for 1700 LT 1–14 Oct. Note that the contour interval is smaller by a factor of 10 in (c). Green shading represents regions of rising motion and yellow shading represents regions of subsidence in (a) and (b).

To facilitate the creation of a 3-h gridded product, when necessary the sounding data were interpolated in time to 3-h resolution as described in Johnson et al. (2015). This time interpolation was needed primarily at Malé and Colombo where the sounding frequency was typically at 6-h resolution. While satellite winds and COSMIC thermodynamic data were used to supplement the soundings as described in Johnson et al. (2015), the gridded analyses shown here are largely independent of any model fields.

To examine the impact of the adjustments on the large-scale analyses, two versions of the gridded analyses described above were created, one without the adjusted soundings and the other with adjustments. Figure 15 shows time series of the surface field changes due to the adjustments at the three island sites as computed from these gridded products. As seen in Fig. 15a, the T changes at Malé are consistently negative reflecting the predominant daytime cooling adjustment at this site (Fig. 13, top panel). The small net positive T change at Gan reflects the slightly larger nighttime warming adjustment at this site (Fig. 13). The moisture changes (Fig. 15b) at Malé and Gan are consistently negative due to the drying adjustments at these sites (Fig. 13, middle panels) while DG periodically shows slight positive changes related primarily to its nighttime moistening adjustment. Surface speed changes (Fig. 15c) are consistently positive and largest at DG, where maxima in speed increases correspond to surges in the u wind (Fig. 15d), which dominates the smaller v wind component (Fig. 15e).

Time–height plots of the changes in the zonal wind and several diagnostic fields resulting from the adjustments are shown (Fig. 16) where fields have been averaged over the NSA (left panels) and southern sounding array (SSA) (right panels). As expected, due to the design of the adjustment procedure changes in zonal wind and divergence are limited to the lowest 200 m of the atmosphere. The switch from low-level divergence to convergence over the SSA in late November is related to the corresponding increase in low-level westerlies at this time. Because vertical motion is computed as a vertical integral of the divergence field, its changes due to the adjustment peak above the boundary layer. Since the structure of apparent heating Q_1 and moistening Q_2 fields are strongly determined the vertical motion, changes in these fields above 200 m are closely tied to boundary layer divergence changes. Within the boundary layer, changes in Q_1 and Q_2 show significant variability on the diurnal time scale and are related to low-level temperature and moisture adjustments described earlier. While changes in the diagnostic fields are generally larger over the SSA due to the larger wind speed adjustments at DG (Figs. 13 and 15), it important to note that these changes are small relative to the magnitude of the fields

themselves—typically representing only a few percent change in the fields.[4] For example, peak changes in Q_2 over the SSA due to the adjustment are ~0.5 K day^{-1} while peaks in time–height Q_2 field are on the order of 10–15 K day^{-1} (see Fig. 6 of Johnson et al. 2015).

To better understand the relationship of the wind adjustments to changes in the diagnosed fields, Fig. 17 shows the adjusted zonal wind speed at the island sites along with the changes in vertically averaged divergence and vertical motion, and Q_2-budget-derived rainfall over the sounding arrays. The most notable signal over the SSA is a systematic shift from low-level divergence to convergence in late November (Fig. 17b). This shift is related to an intraseasonal zonal wind change from easterlies to westerlies at Gan and DG during this period (Fig. 17a), since enhanced low-level westerlies at these sites on the western boundary of the SSA lead to enhanced low-level convergence over this region. This in turn results in increased upward motion (Fig. 17c), and the observed increase in SSA rainfall (Fig. 17d). The greatest impact over the NSA due to the adjustment also occurs in late November when an increase in westerlies at Malé and Gan during the active phase of an MJO results in a week-long increase in low-level convergence over the NSA, and consequently, enhanced upward motion and increased rainfall. The peak rainfall increases noted here (0.3–0.5 mm day^{-1}) over the arrays represent ~4% increase to the long-term array means [~9.0 mm day^{-1} estimated by the TRMM 3B42 product as reported in Johnson et al. (2015)]. In comparison, the impact of the adjustments at Colombo, which were made over a much deeper layer (i.e., from the surface to 3 km), increased NSA rainfall by ~11% of the SOP-mean with the largest increase of ~3 mm day^{-1} (or 38%) during a 2-week period of the November MJO build-up phase (Ciesielski et al. 2014b).

The enhanced westerlies over the NSA and stronger easterlies at DG during the first half of October result in opposing changes in the low-level divergence, omega, and rainfall between the arrays (Fig. 17). The circulation during this period was characterized by a local Hadley cell with suppressed convection over the NSA and strong upward motion and ITCZ convection across the southern portion of the SSA (Ciesielski et al. 2018). A prominent diurnal pulsing of this cell was observed with the cell running strongest during the early morning hours (0500–0800 LT) and notably weakening (up to 50%) later in the day (1700–2000 LT). To investigate the impact of the adjustment on the strength of this cross-equatorial cell, Fig. 18 shows the north–south cross section of vertical motion for this two-week period at 1700 LT, which is the time of day when the impact was a maximum. As seen here, the increased low-level convergence over the NSA results in decreased subsidence there (green shaded area in Fig. 18c), while the increased low-level divergence over the SSA causes a slight reduction in upward motion (yellow shaded area). As a result, the local Hadley circulation is weakened ~7% at 1700 LT when the impact is most pronounced and about 5% in the daily mean.

[4] The mean and temporal behavior of these diagnostic fields for the DYNAMO period can be found in Johnson et al. (2015).

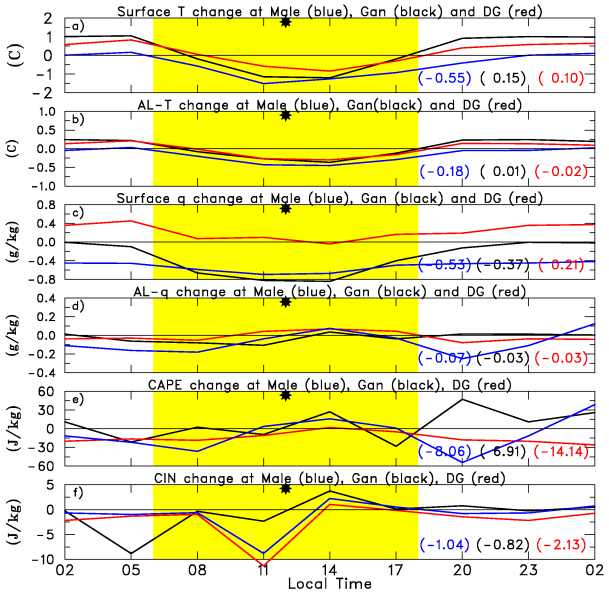

FIG. 19. Diurnal cycle of changes in (a) surface T, (b) AL T, (c) surface q, (d) AL q, (e) CAPE, and (f) CIN for Malé (blue), Gan (black), and DG (red). Note that the y scales for the surface plots [(a),(c)] span 2 times the range for the AL plots [(b),(d)]. The numbers in parentheses show the period means. Daytime hours are highlighted in yellow, and asterisks denote local noon.

In short, these small impacts do not alter the conclusion of the previous work on the significance of the cross-equatorial Hadley cell and its diurnal pulsing during the early October period of DYNAMO.

Because of the sensitivity of convection to boundary layer thermodynamic quantities, we consider the impact of the adjustment on some basic convective parameters. Here CAPE and CIN were calculated assuming pseudoadiabatic ascent using mean thermodynamic conditions in the lowest 50 hPa. While changes in the time-mean values of the CAPE and CIN averaged less than 1% and 3%, respectively, Fig. 19 considers their changes over the diurnal cycle since the adjustments varied diurnally. Shown here is the change of T and q at the surface as well as their average in the layer from the surface to 200 m, referred to here as the adjustment layer (AL). While the AL temperature diurnal cycle shows a similar behavior to the surface diurnal cycle except with about half the amplitude (Figs. 19a,b), the AL moisture diurnal cycle is quite different from that at the surface. For example, all sites show a 1400 LT drying in surface q change due to the adjustment (Fig. 19c), while the AL q shows a slight moistening (Fig. 19d). This behavior is related to the tendency for a drier air layer to lie atop a moist surface layer (see examples in Fig. 11) such that a dying adjustment at the surface is often associated with a moistening adjustment in the layer above. The diurnal CAPE and CIN changes are moderated by the fact that positive (negative) T changes are generally compensated by negative (positive) q changes. A few notable exceptions to this are at Gan where nighttime (2000–0200 LT) changes in T and q are both positive, resulting in 30–50 J kg^{-1} CAPE increases, and

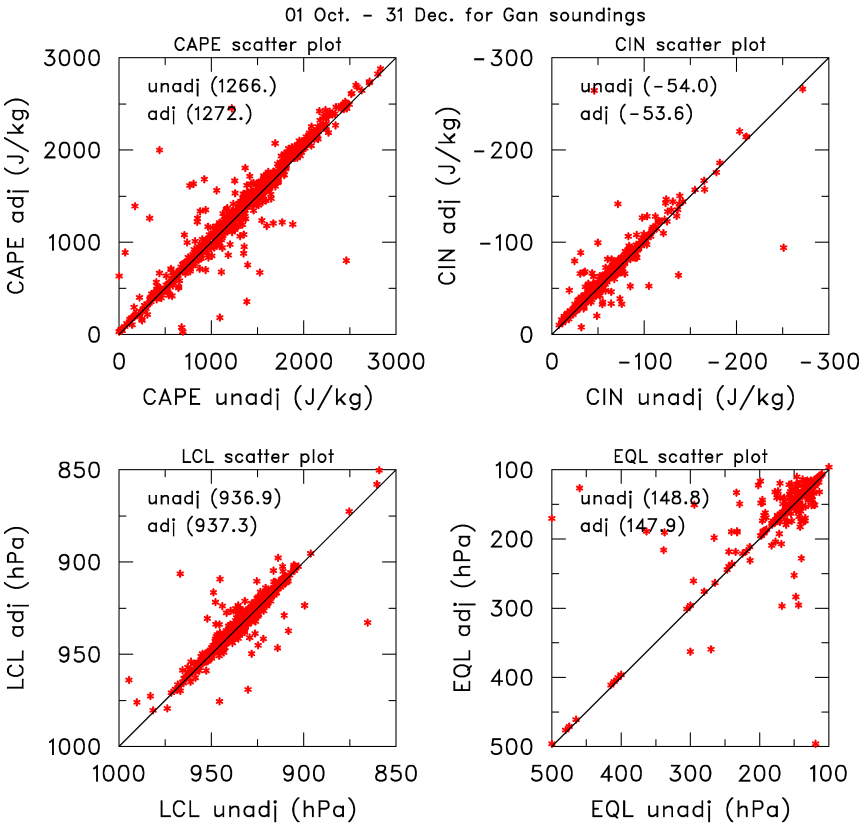

FIG. 20. Scatterplot of convective parameters at Gan for (top left) CAPE, (top right) CIN, (bottom right) EQL, and (bottom left) LCL. Values are computed from adjusted soundings plotted along the *y* axis vs values from unadjusted sounding along the *x* axis. The numbers in parentheses refer to period means.

at Malé at 2000 LT where T and q changes are both negative, resulting in a 60 J kg^{-1} reduction in CAPE (Fig. 19e). Even these more significant changes in CAPE at specific times of day represent only a 3%–4% change from the daily mean.

A scatterplot of adjusted versus unadjusted values of convection parameters for Gan is shown in Fig. 20. In addition to CAPE and CIN this figure also shows the impact of the adjustment on the lifting condensation level (LCL) and level of neutral buoyancy or equilibrium level (EQL). At Gan, the percentage changes[5] of CAPE and CIN due to the adjustment averaged over all soundings are 8.8% and 7.2%, respectively, which is slightly higher than at the other sites. Viewed another way, the low-level adjustments of T and q resulted in CAPE and CIN percentage changes >10% in 16% of the soundings at Gan (15% at DG and 9% at Malé). So, while mean CAPE and CIN changes due to the adjustment were small, adjustments at individual times occasionally resulted in substantial changes in these parameters as evidenced by the points in the scatterplot away from the 1-to-1 line.

[5] The percentage change is defined as the change in a value due to the adjustment divided by its original value.

5. Summary

During the DYNAMO field campaign, upper-air soundings were routinely launched from three small islands/atolls (Malé, Gan, and Diego Garcia) located on the western boundary of the enhanced sounding network. On several occasions during this experiment, dropsondes were made in the near vicinity of Gan and Diego Garcia. Comparisons of island upsondes to nearby and proximity dropsondes over the ocean provide evidence for the islands' influence on the surrounding atmosphere and on the island upsonde profiles. Island effects, including near-surface daytime heating and nighttime cooling, as well as wind speed reduction due to enhanced friction over land, are most prominent in the lowest 200 m, but on some occasions these effects extend even higher (up to 600 m). Because of the large spacing between the sounding sites (~500–700 km), aliasing of these local island effects onto larger scales is possible, thereby effecting the computation of atmospheric budgets (Ciesielski et al. 2014b). This study applies an adjustment procedure to mitigate these island effects and examines the impact of the adjustments on various analyses.

Noting from the dropsonde profiles that the vertical gradients of temperature, moisture, and wind speed over the ocean are generally constant in the lowest 0.5 km, a simple

procedure was constructed to adjust the upsonde profiles in the lowest few hundred meters to resemble the atmospheric structures over the open ocean, and, in effect, to mitigate the islands' influence on the data. In this procedure average vertical gradients of temperature, moisture, and winds computed in the upper portion of the atmospheric boundary layer (typically above 200 m) were extrapolated to surface. To account for situations where island winds were localized and not representative of the larger scale, a second step was added to further adjust the low-level wind direction. For this step ECMWF operational analysis winds sampled at a 1° radius around the island sounding sites were objectively analyzed to the sounding locations and then blended with island sounding wind direction data at low levels. This adjustment procedure was applied to the soundings from the three islands mentioned above for the October–December 2011 period of DYNAMO.

As a result of this procedure, daytime (nighttime) low-level temperatures are cooled (warmed) such that their adjusted diurnal cycle amplitude at the surface is reduced fivefold, resembling that over the ocean as observed from DYNAMO ship observations. In addition, the procedure increases the low-level wind speeds in ~90% of the island soundings. The largest low-level wind changes due to the adjustment were at Diego Garcia, where the 3-month mean surface wind speed increase was 3.7 m s^{-1}. The mean surface wind speed biases (model-adjusted soundings) at the island sites are quite similar to those at the open-ocean sites (i.e., the R/V *Revelle* and R/V *Mirai*), lending credibility to the wind speed adjustments.

Examination of the impact of these sounding adjustments shows that dynamical (i.e., divergence and vertical motion) and budget (Q_1 and Q_2) fields are primarily affected by adjustments to the wind field, while, as one would expect, convective parameters are sensitive to the adjustments in thermodynamic fields. Although the impact of the adjustments is generally small on diagnosed fields (order a few percent), intraseasonal wind regime changes result in some systematic variations in the large-scale fields and an increase to the SSA rainfall during December period on the order of 4% of the 3-month mean. Also, during the first half of October, characterized by suppressed MJO conditions over and north of the equator and ITCZ convection over the southern half of the SSA, the adjustments resulted in a weakening of the cross-equatorial Hadley cell by about 5%. The impact of the adjustment on the convective parameters is small in a mean sense (1%–3%); however, ~15% of the soundings show significant (>10%) changes in CAPE and CIN values. Even these more noteworthy impacts of the adjustment are still quite small, and as such, have little effect on the MJO budget analyses over the DYNAMO arrays as presented in earlier studies (e.g., Johnson and Ciesielski 2013; Johnson et al. 2015).

As seen in some of the upsonde comparisons to nearby dropsonde data, the impact of these small islands on the surrounding atmosphere can at times extend to beyond 200 m. However, trying to identify these cases and mitigate these deeper island effects is difficult without additional data. Having nearby island dropsondes representative of open-ocean conditions on a regular basis would greatly help to identify the extent and frequency of these deeper island effects. Despite the limitations of the adjustment procedure, this study provides a first attempt to estimate the magnitude of the impact of using small islands or atolls for sounding platforms, often unavoidable in field campaigns, on errors in diagnosed fields over large-scale sounding arrays.

Acknowledgments. We thank Wayne Schubert for many insightful discussions, Richard Taft for his help with many of the figures, and two anonymous reviewers for their constructive comments. We also acknowledge the efforts of Qing Wang and Shuyi Chen for their excellent coordination of the NOAA P3 dropsonde missions. This research was supported by the National Science Foundation (NSF) under Grant AGS-1853633.

Data availability statement. The TRMM 3B42 rainfall data were obtained from http://mirador.gsfc.nasa.gov/, the legacy sounding products are from https://data.eol.ucar.edu/project/DLDP, the ECMWF operational analyses are from https://data.eol.ucar.edu/master_lists/generated/dynamo/, and the CSU gridded analyses are from http://johnson.atmos.colostate.edu/dynamo/products/gridded/.

REFERENCES

Ciesielski, P. E., and Coauthors, 2014a: Quality-controlled upper-air sounding dataset for DYNAMO/CINDY/AMIE: Development and corrections. *J. Atmos. Oceanic Technol.*, **31**, 741–764, https://doi.org/10.1175/JTECH-D-13-00165.1.

——, R. H. Johnson, K. Yoneyama, and R. K. Taft, 2014b: Mitigation of Sri Lanka island effects in Colombo sounding data and its impact on DYNAMO analyses. *J. Meteor. Soc. Japan*, **92**, 385–405, https://doi.org/10.2151/jmsj.2014-407.

——, ——, W. H. Schubert, and J. H. Ruppert Jr., 2018: Diurnal cycle of the ITCZ in DYNAMO. *J. Climate*, **31**, 4543–4562, https://doi.org/10.1175/JCLI-D-17-0670.1.

Daley, E. L., 2012: The effects of a remote atoll and lagoon on the marine boundary layer. M.S. thesis, Dept. of Meteorology, Naval Postgraduate School, 56 pp.

Fine, C. M., R. H. Johnson, P. E. Ciesielski, and R. K. Taft, 2016: The role of topographically induced vortices in tropical cyclone formation over the Indian Ocean. *Mon. Wea. Rev.*, **144**, 4827–4847, https://doi.org/10.1175/MWR-D-16-0102.1.

Huffman, G. J., and Coauthors, 2007: The TRMM multi-satellite precipitation analysis: Quasi-global, multi-year, combined-sensor precipitation estimates at fine scale. *J. Hydrometeor.*, **8**, 38–55, https://doi.org/10.1175/JHM560.1.

Johnson, R. H., and P. E. Ciesielski, 2013: Structure and properties of Madden–Julian oscillations deduced from DYNAMO sounding arrays. *J. Atmos. Sci.*, **70**, 3157–3179, https://doi.org/10.1175/JAS-D-13-065.1.

——, and ——, 2017: Multiscale variability of the atmospheric boundary layer during DYNAMO. *J. Atmos. Sci.*, **74**, 4003–4021, https://doi.org/10.1175/JAS-D-17-0182.1.

——, ——, and J. A. Cotturone, 2001: Multiscale variability of the atmospheric mixed-layer over the western Pacific warm pool. *J. Atmos. Sci.*, **58**, 2729–2750, https://doi.org/10.1175/1520-0469(2001)058<2729:MVOTAM>2.0.CO;2.

——, ——, J. H. Ruppert Jr., and M. Katsumata, 2015: Sounding-based thermodynamic budgets for DYNAMO. *J. Atmos. Sci.*, **72**, 598–622, https://doi.org/10.1175/JAS-D-14-0202.1.

Long, C. N., and S. A. McFarlane, 2011: Quantification of the impact of Nauru Island on ARM measurements. *J. Appl. Meteor. Climatol.*, **51**, 628–636, https://doi.org/10.1175/JAMC-D-11-0174.1.

Matthews, S., J. M. Hacker, J. Cole, J. Hare, C. N. Long, and R. M. Reynolds, 2007: Modification of the atmospheric boundary layer by a small island: Observations from Nauru. *Mon. Wea. Rev.*, **135**, 891–905, https://doi.org/10.1175/MWR3319.1.

McFarlane, S. A., C. N. Long, and D. M. Flynn, 2005: Impact of island-induced clouds on surface measurements: Analysis of the ARM Nauru Island Effects Study data. *J. Appl. Meteor.*, **44**, 1045–1065, https://doi.org/10.1175/JAM2241.1.

Mori, S., and Coauthors, 2004: Diurnal land–sea rainfall peak migration over Sumatra Island, Indonesian maritime continent, observed by TRMM satellite and intensive rawinsonde soundings. *Mon. Wea. Rev.*, **132**, 2021–2039, https://doi.org/10.1175/1520-0493(2004)132<2021:DLRPMO>2.0.CO;2.

Nagarajan, B., and A. Aiyyer, 2004: Performance of the ECMWF operational analyses over the tropical Indian Ocean. *Mon. Wea. Rev.*, **132**, 2275–2282, https://doi.org/10.1175/1520-0493(2004)132<2275:POTEOA>2.0.CO;2.

Nuss, W. A., and D. W. Titley, 1994: Use of multiquadric interpolation for meteorological objective analysis. *Mon. Wea. Rev.*, **122**, 1611–1631, https://doi.org/10.1175/1520-0493(1994)122<1611:UOMIFM>2.0.CO;2.

Praveen Kumar, B., J. Vialard, M. Lengaigne, V. S. N. Murty, and M. J. McPhaden, 2012: TropFlux: Air-sea fluxes for the global tropical oceans—Description and evaluation. *Climate Dyn.*, **38**, 1521–1543, https://doi.org/10.1007/s00382-011-1115-0.

Smith, R. B., and V. Grubisic, 1993: Aerial observations of Hawaii's wake. *J. Atmos. Sci.*, **50**, 3728–3750, https://doi.org/10.1175/1520-0469(1993)050<3728:AOOHW>2.0.CO;2.

Vömel, H., and Coauthors, 2007: Radiation dry bias of the Vaisala RS92 humidity sensor. *J. Atmos. Oceanic Technol.*, **24**, 953–963, https://doi.org/10.1175/JTECH2019.1.

Wang, S., and A. H. Sobel, 2017: Factors controlling rain on small tropical islands: Diurnal cycle, large-scale wind speed, and topography. *J. Atmos. Sci.*, **74**, 3515–3532, https://doi.org/10.1175/JAS-D-16-0344.1.

Weckwerth, T., T. W. Horst, and J. W. Wilson, 1999: An observational study of the evolution of horizontal convective rolls. *Mon. Wea. Rev.*, **127**, 2160–2179, https://doi.org/10.1175/1520-0493(1999)127<2160:AOSOTE>2.0.CO;2.

Yanai, M., S. Esbensen, and J.-H. Chu, 1973: Determination of bulk properties of tropical cloud clusters from large-scale heat and moisture budgets. *J. Atmos. Sci.*, **30**, 611–627, https://doi.org/10.1175/1520-0469(1973)030<0611:DOBPOT>2.0.CO;2.

Yoneyama, K., M. Hanyu, F. Yoshiura, S. Sueyoshi, and M. Katsumata, 2002: Radiosonde observation from the ship in the tropical region. Japan Marine Science and Technology Center. Rep. 45, 31–39, http://www.jamstec.go.jp/dcop/e/publications/pdf/Yoneyama-etal_2002_JAMSTECR.pdf.

——, C. Zhang, and C. N. Long, 2013: Tracking pulses of the Madden–Julian oscillation. *Bull. Amer. Meteor. Soc.*, **94**, 1871–1891, https://doi.org/10.1175/BAMS-D-12-00157.1.